M. Pouagare
Graduate Assistant.

B. Lakshminarayana
Director of Computational Fluid Dynamics Studies and Professor of Aerospace Engineering.

Department of Aerospace Engineering,
The Pennsylvania State University,
University Park, Pa. 16802

Development of Secondary Flow and Vorticity in Curved Ducts, Cascades, and Rotors, Including Effects of Viscosity and Rotation

This paper is concerned with the numerical solution of the secondary vorticity equations in curved ducts, cascades, and rotors. The classical approach of splitting the flow into primary and secondary flow fields is employed and extended to include effects of viscosity, rotation, and density stratification. All elliptical effects are neglected and the Crank-Nicolson method is used to solve the secondary vorticity equation. The secondary flow field is obtained by solving a Poisson equation using a successive over-relaxation method. The results are compared with theoretical and experimental data from stationary ducts, compressor and turbine cascades. The agreement is good for most of the cases.

Introduction

Secondary flow is produced when a streamwise component of vorticity is developed from the deflection of an initially sheared flow. Such secondary flows occur when a developed pipe flow enters a bend or cascade or a rotor, or when a boundary layer meets an obstacle normal to the surface over which it is flowing. One of the most important engineering aspects of secondary flow occurs in turbomachinery aerodynamics, where boundary layers growing on the casing and hub walls of the machine are deflected by rows of blades, stationary and rotating. At a sufficient distance from the walls, viscous effects are negligible and the normal pressure gradient is balanced by the centrifugal force due to the streamline curvature. However, the fluid within the boundary layers does not have sufficient momentum to balance the pressure gradients imposed by the inviscid outer flow. The result is a cross-flow component containing vorticity aligned in the streamwise direction. This results in flow losses, vorticity development, and flow deviation in the tangential and radial directions. The efficiency of the rotor is also affected by this secondary flow.

The primary assumption leading to the existing theoretical descriptions of secondary flows is that viscous effects produce a boundary layer on the wall upstream of the blade row, whereas within the blade row the imposed pressure gradients play the major role and viscosity has little effect on the resulting secondary flows. This assumption is characteristic of what is generally termed inviscid secondary flow analysis or "classical secondary flow theory" [1, 2, 3]. All these earlier analyses, reviewed in reference [3], are based on assumptions that the flow perturbations occur mainly in the cross section of the bend or cascade and that the perturbations due to secondary flow in the streamwise direction are small. This linearization approach uncouples the primary and secondary flow fields.

In general, these linearized theories provide accurate prediction of the spanwise exit-flow angle for the small turning angle in the inviscid regions. When features of the real flow are modelled, i.e., Bernoulli surface displacement, rotation, and viscous effects, the overturning near the end wall is reduced [4].

An exact approach would be to solve, numerically, the entire viscid or inviscid equations which do not uncouple the primary and secondary flow fields. Such attempts are presently being pursued by several groups [5–9]. However, these methods are quite complicated and time-consuming. The advantage of the classical approach lies in its simplicity. The objective of this paper is to extend the classical approach

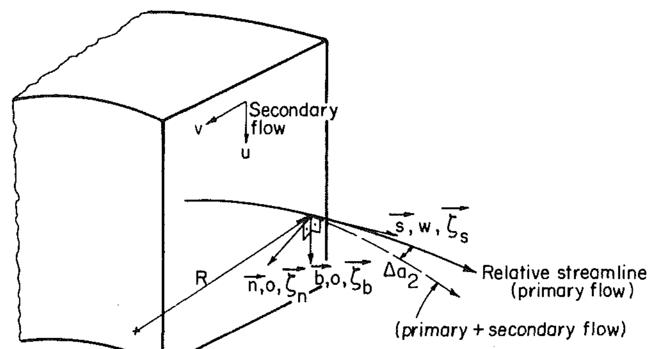

Fig. 1 Notations used and the coordinate system

Contributed by the Fluids Engineering Division and presented at the AIAA/ASME Joint Fluids, Plasma, Thermophysics and Heat Transfer Conference, St. Louis, Mo., June 7–11, 1982, of THE AMERICAN SOCIETY OF MECHANICAL ENGINEERS. Manuscript received by the Fluids Engineering Division, October 28, 1981.

by introducing the effects of viscosity, rotation, and inlet density gradients on the development of the secondary vorticity in curved duct and turbomachine blade passages. The agreement between the predictions from this analysis and several experimental data is shown to be good.

Analysis

The most generalized form of the equations for the secondary and normal vorticity in a rotating intrinsic coordinate system was developed by Lakshminarayana and Horlock in reference [10]. The coordinate system used is shown in Fig. 1. s is the relative streamline direction, n is the principle normal to the streamline direction, and b is the binormal direction. s, n, b form an orthogonal coordinate system.

The relative secondary vorticity ζ_s and the relative normal vorticity ζ_n along the relative streamline are given, respectively, by the following equations [10]

$$\frac{\partial}{\partial s}\left(\frac{\zeta_s}{\rho w}\right)=\frac{2\zeta_n}{\rho w R}+\frac{2\Omega_s}{\rho^2 w}\frac{\partial \rho}{\partial s}-\frac{1}{\rho^3 w^2}\left[\frac{\partial \rho}{\partial b}\frac{\partial P}{\partial n}-\frac{\partial \rho}{\partial n}\frac{\partial P}{\partial b}\right]$$
$$+\frac{2\mathbf{\Omega}\cdot\nabla w}{\rho w^2}+\frac{\mu}{\rho^2 w^2}\mathbf{s}\cdot\nabla^2\boldsymbol{\zeta}-\frac{1}{\rho w^2}\mathbf{s}\cdot\nabla\left(\frac{\mu}{\rho}\right)\times\nabla\times\boldsymbol{\zeta}$$
$$+\frac{4}{3}\frac{1}{\rho w^2}\mathbf{s}\cdot\nabla\left(\frac{\mu}{\rho}\right)\times\nabla(\nabla\cdot\mathbf{w}) \qquad (1)$$

$$\frac{\partial}{\partial s}(\zeta_n w)=\frac{w}{\tau}\zeta_b-\frac{w}{a_b}\frac{\partial a_b}{\partial s}(\zeta_n+2\Omega_n)+\frac{2\Omega_s w}{R}-2\Omega_n\frac{\partial w}{\partial s}$$
$$+\frac{1}{\rho^2}\left[\frac{\partial P}{\partial s}\frac{\partial \rho}{\partial b}-\frac{\partial P}{\partial b}\frac{\partial \rho}{\partial s}\right]+\mathbf{n}\cdot\frac{\mu}{\rho}\nabla^2\boldsymbol{\zeta}$$
$$-\mathbf{n}\cdot\nabla\left(\frac{\mu}{\rho}\right)\times\nabla\times\boldsymbol{\zeta}+\frac{4}{3}\mathbf{n}\cdot\left(\nabla\left(\frac{\mu}{\rho}\right)\times\nabla(\nabla\cdot\mathbf{w})\right) \qquad (2)$$

For an incompressible stratified fluid in b direction, the above equations simplify to

$$\frac{\partial}{\partial s}\left(\frac{\zeta_s}{w}\right)=\frac{2\zeta_n}{wR}-\frac{1}{\rho^2 w^2}\frac{\partial \rho}{\partial b}\frac{\partial P}{\partial n}$$
$$+\frac{2\mathbf{\Omega}\cdot\nabla w}{w^2}+\frac{\mu}{\rho w^2}\mathbf{s}\cdot\nabla^2\boldsymbol{\zeta} \qquad (3)$$

$$\frac{\partial}{\partial s}(\zeta_n w)=\frac{w}{\tau}\zeta_b-\frac{w}{a_b}\frac{\partial a_b}{\partial s}(\zeta_n+2\Omega_n)+\frac{2\Omega_s w}{R}-2\Omega_n\frac{\partial w}{\partial s}$$
$$+\frac{1}{\rho^2}\frac{\partial P}{\partial s}\frac{\partial e}{\partial b}+\mathbf{n}\cdot\frac{\mu}{\rho}\nabla^2\boldsymbol{\zeta} \qquad (4)$$

These equations will be solved in the region close to the wall where the inlet vorticity is present, i.e., in the boundary layer region.

Employing the usual boundary layer approximations, it is assumed that the pressure is imposed by the inviscid flow field and that the viscous effects are important only in the direction normal to the wall, i.e., in the b direction. So we can set

$$\frac{\partial P}{\partial n}=\frac{\partial P_0}{\partial n}=-\rho\frac{W_0^2}{R}$$

$$\mathbf{s}\cdot\frac{\mu}{\rho w^2}\nabla^2\boldsymbol{\zeta}=\frac{\mu}{\rho w^2}\frac{\partial^2\zeta_s}{\partial b^2}$$

$$\mathbf{n}\cdot\frac{\mu}{\rho}\nabla^2\boldsymbol{\zeta}=\frac{\mu}{\rho}\frac{\partial^2\zeta_n}{\partial b^2}$$

Furthermore, we can write

$$\frac{2\mathbf{\Omega}\cdot\nabla w}{w^2}=\frac{2}{w^2}\left(\Omega_s\frac{\partial w}{\partial s}+\Omega_n\frac{\partial w}{\partial n}+\Omega_b\frac{\partial w}{\partial b}\right)$$

In most practical situations, ζ_b is zero. Hence, $\partial w/\partial n = w/R$. Also, $\zeta_n = \partial w/\partial b$. Hence,

$$\frac{2\mathbf{\Omega}\cdot\nabla w}{w^2}=\frac{2}{w^2}\left(\Omega_s\frac{\partial w}{\partial s}+\Omega_n\frac{w}{R}+\Omega_b\zeta_n\right)$$

Assuming $\partial a_b/\partial s = 0$, and noting that the first term on the right side of equation (4) is very small (since $\zeta_b \approx 0$ and τ is usually very large with these assumptions), equations (3) and (4) reduce to,

Nomenclature

a_b = relative streamline spacing in the b direction
b_0 = height of the blades/height of the duct
P = static pressure
R = radius of curvature of relative streamline
$R_e=\dfrac{W_1\cdot\delta_1\cdot\rho_1}{\mu}$ = Reynolds number
S = width of the duct (or spacing in cascade)
s,n,b = intrinsic coordinate system (Fig. 1)
u,v = secondary velocities in b, n directions, respectively (Fig. 1)
w = relative velocity inside the shear layer
W_0 = free stream relative velocity
W_1 = free stream relative velocity at inlet
β = relative air angle measured from the axial direction
δ = boundary layer thickness
δ^* = boundary layer displacement thickness
ζ = relative vorticity/absolute vorticity for $\Omega = 0$
λ = stagger angle
μ = molecular viscosity
μ_e',μ_e'',μ_e = eddy viscosity (equations (10) and (11))
ν = kinematic viscosity
ρ = density
ρ_1 = reference density
τ = radius of torsion of the streamline
τ_0 = wall shear stress
ψ = secondary stream function
Ω = angular velocity
$\Delta s,\Delta n,\Delta b$ = stepsize in s,n,b direction
$\Delta\alpha_2$ = change in outlet angle due to secondary vorticity

Subscripts

s,n,b = components in intrinsic coordinate system
0 = reference/inviscid/free stream values
1 = inlet of the blade row
2 = outlet of the blade row

Superscripts

—— = nondimensional quantities/passage averaged quantities/time averaged quantities
bold face = vector

$$\frac{\partial}{\partial s}\left(\frac{\zeta_s}{w}\right)=\frac{2\zeta_n}{wR}+\frac{W_0^2}{\rho w^2 R}\frac{\partial \rho}{\partial b}+\frac{2}{w^2}\left(\Omega_s\frac{\partial w}{\partial s}+\Omega_n\frac{w}{R}+\Omega_b\zeta_n\right)+\frac{\mu}{\rho w^2}\frac{\partial^2\zeta_s}{\partial b^2} \quad (5)$$

$$\frac{\partial}{\partial s}(\zeta_n w)=\frac{2\Omega_s w}{R}-2\Omega_n\frac{\partial w}{\partial s}+\frac{1}{\rho^2}\frac{\partial P_0}{\partial s}\frac{\partial \rho}{\partial b}+\frac{\mu}{\rho}\frac{\partial^2\zeta_n}{\partial b^2} \quad (6)$$

Equations (5) and (6) are valid for laminar flow. In case of turbulent flow the last term in equations (5) and (6) become, respectively,

$$\frac{1}{\rho w^2}\frac{\partial^2}{\partial b^2}\left[(\mu+\mu_e)\zeta_s\right] \quad , \quad \frac{1}{\rho}\frac{\partial^2}{\partial b^2}\left[(\mu+\mu_e)\zeta_n\right]$$

The derivation of these terms are given in Appendix 1.

One of the major assumptions of the present method is that the streamwise $w(s,b)$ velocity profile is assumed known. Since no boundary layer growth is allowed, it is reasonable to neglect the viscous term in the normal vorticity equation.

Equations (5) and (6) are nondimensionalized using the free stream velocity (W_1) at the inlet as the characteristic velocity, the inlet boundary layer thickness δ_1 as the characteristic length, and some reference density ρ_1. The boundary layer growth through the duct or blade row is neglected.

$$\bar{\zeta}=\zeta\frac{\delta_1}{W_1},\ \bar{\Omega}=\Omega\frac{\delta_1}{W_1},\ \bar{w}=\frac{w}{W_1},\ \bar{W}_0=\frac{W_0}{W_1},\ \bar{P}=\frac{P}{\rho_1 W_1^2},$$

$$\bar{\rho}=\frac{\rho}{\rho_1},\ \bar{s}=\frac{s}{\delta_1},\ \bar{b}=\frac{b}{\delta_1},\ \bar{n}=\frac{n}{\delta_1},\ \bar{R}=\frac{R}{\delta_1},$$

$$\bar{\psi}=\frac{\psi}{W_1\delta_1},\ \bar{\mu}=\frac{\mu_e+\mu}{\mu}$$

The resulting equations are given by

$$\frac{\partial}{\partial \bar{s}}\left(\frac{\bar{\zeta}_s}{\bar{w}}\right)=\underset{1}{\frac{2\bar{\zeta}_n}{\bar{w}\bar{R}}}+\underset{2}{\frac{2}{\bar{w}^2}\left(\bar{\Omega}_s\frac{\partial \bar{w}}{\partial \bar{s}}+\bar{\Omega}_n\frac{\bar{w}}{\bar{R}}+\bar{\Omega}_b\bar{\zeta}_n\right)}+\underset{3}{\frac{1}{\bar{\rho}\bar{w}^2}(\bar{W}_0)^2\frac{1}{\bar{R}}\frac{\partial\bar{\rho}}{\partial\bar{b}}}+\underset{4}{\frac{1}{\mathrm{Re}}\frac{1}{\bar{\rho}\bar{w}^2}\frac{\partial^2}{\partial\bar{b}^2}[\bar{\mu}\,\bar{\zeta}_s]} \quad (7)$$

$$\frac{\partial}{\partial\bar{s}}(\bar{\zeta}_n\bar{w})=\underset{1}{\frac{2\bar{\Omega}_s\bar{w}}{\bar{R}}}-\underset{2}{2\bar{\Omega}_n\frac{\partial\bar{w}}{\partial\bar{s}}}+\underset{3}{\frac{1}{\bar{\rho}^2}\frac{\partial\bar{P}_0}{\partial\bar{s}}\frac{\partial\bar{\rho}}{\partial\bar{b}}} \quad (8)$$

where

$$\mathrm{Re}=\frac{W_1\bullet\delta_1\bullet\rho_1}{\mu}$$

Equations (7) and (8) can be solved for the values of $\bar{\zeta}_n$ and $\bar{\zeta}_s$ at any given location. Since these equations are decoupled, the value of $\bar{\zeta}_n$ can be derived from the solution of equation (8), which can then be substituted in equation (7) to derive the value of $\bar{\zeta}_s$. Solution of the inviscid terms of these equations is available for many simpler cases [1-4, 10], but the numerical or analytical solution of the streamwise and normal vorticity equations with the viscous terms has never been attempted before.

Knowing the value of $\bar{\zeta}_s$ along the mean streamline, the secondary velocities $\bar{u}$, $\bar{v}$ in the transverse plane can be derived from the numerical solution of the Poisson's equation for the secondary stream function

$$\nabla^2\bar{\psi}=-\bar{\zeta}_s(\bar{b},\bar{n}) \quad (9)$$

where $\bar{u}$ and $\bar{v}$ are perturbation velocities (from initially zero values in the primary flow) in b and n directions. Expressions for these are given respectively, by

$$\bar{u}=\frac{u}{W_1}=-\frac{\partial\bar{\psi}}{\partial\bar{n}} \quad , \quad \bar{v}=\frac{v}{W_1}=\frac{\partial\bar{\psi}}{\partial\bar{b}}$$

where $\bar{b}$ and $\bar{n}$ are rectilinear coordinates.

The change in the outlet angle (or deviation angle from the primary flow) can be obtained from the equation

$$\Delta\alpha_2=\tan^{-1}\frac{\bar{v}}{\bar{w}}$$

It should be emphasized that the calculation procedure outlined here assumes that the primary flow is known $[w(b,n,s)]$. Utilizing this value and equations (7), (8), and (9), the secondary vorticity $(\bar{\zeta}_s)$, normal vorticity $(\bar{\zeta}_n)$, and secondary velocities $(\bar{u}, \bar{v})$ are calculated. In the numerical scheme presented in the next section, it is assumed that the secondary vorticity is constant in the $\bar{n}$ direction (which is true in most practical situations), hence $\bar{\zeta}=\bar{\zeta}(b)$, and the equations are solved in the $(\bar{s}\ \bar{b})$ plane along the mean streamline using a marching technique. The mean streamline is the streamline at the mid-passage and is the mean (vectorial) between the streamlines near the pressure and suction surfaces.

Turbulence Closure. To study the effect of turbulence in the development of secondary flow, eddy viscosity is used in equation (7). The eddy viscosity is modelled as follows [11]:

for $0 \le b \le b_k$

$$\mu_e'=\rho\left\{kb\left[1-\exp\left(-\frac{b\sqrt{\tau_0/\rho}}{\nu A}\right)\right]\right\}^2\frac{\partial w}{\partial b} \quad (10)$$

for $b_k \le b \le \delta$

$$\mu_e''=\rho k_2 W_0\delta^*/[1+5.5(b/\delta)^6] \quad (11)$$

where A, k, and k_2 are constants, given by values $k = 0.4$, $A = 26$, and $k_2 = 0.017$.

The value of b_k which delineates the range of validity of equation (10) from equation (11) is obtained from the requirement that the eddy viscosities must assume equal values there. Hence,

$$\mu_e'=\mu_e'' \quad \text{for} \quad b=b_k$$

Numerical Solution and Boundary Conditions

Equations (7) and (8) are solved along the mean streamline of the duct or the blade passage in the boundary layer region. The solution is marched in the downstream direction using Crank-Nicolson method. This procedure neglects any elliptical effects. This assumption is good provided there is no flow separation. The streamwise velocity profile (primary flow) is assumed to be known.

The s coordinate is the time-like variable. The equations are approximated at the location $(i+1/2, j)$, where the index i is the mesh point in the streamwise direction and j is the mesh point in the b direction. Since equation (8) is uncoupled from equation (7), the value of $(\bar{\zeta}_n)_{i+1,j}$ can be evaluated from the known value. The rest of the quantities in equation (8) are known either from the primary flow solution, geometry, or the fluid properties. The finite difference form of equations (7) and (8) are, respectively,

$$-A_1(\bar{\zeta}_s)_{i+1,j-1}+(B_1+2A_2)(\bar{\zeta}_s)_{i+1,j}-A_3(\bar{\zeta}_s)_{i+1,j+1}=A_4(\bar{\zeta}_s)_{i,j-1}+(B_2-2A_5)(\bar{\zeta}_s)_{i,j}+A_6(\bar{\zeta}_s)_{i,j+1}+C_1 \quad (12a)$$

$$B_3(\bar{\zeta}_n)_{i+1,j}=B_4(\bar{\zeta}_n)_{i,j}+C_2 \quad (12b)$$

Constants A_1-A_6, B_1, B_2 and C in the difference equation (12a) are given by

$$A_1=\left[\frac{1}{\mathrm{Re}\ \bar{\rho}\bar{w}^2}\right]_{i+1/2,j}\frac{\bar{\mu}_{i+1,j-1}}{2(\Delta\bar{b})^2}$$

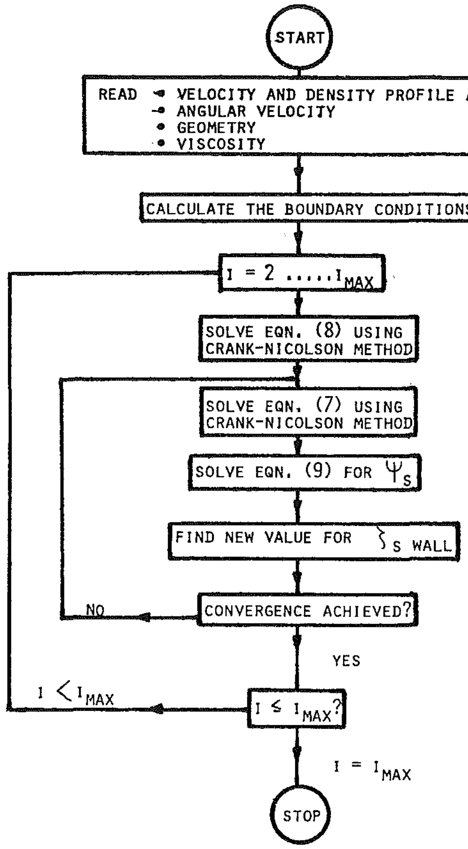

Fig. 2 Flow chart of the computer program

$$A_2 = \left[\frac{1}{\mathrm{Re}\ \bar{\rho}\bar{w}^2}\right]_{i+1/2,j} \frac{\bar{\mu}_{i+1,j}}{2(\Delta\bar{b})^2}$$

$$A_3 = \left[\frac{1}{\mathrm{Re}\ \bar{\rho}\bar{w}^2}\right]_{i+1/2,j} \frac{\bar{\mu}_{i+1,j-1}}{2(\Delta\bar{b})^2}$$

$$A_4 = \left[\frac{1}{\mathrm{Re}\ \bar{\rho}\bar{w}^2}\right]_{i+1/2,j} \frac{\bar{\mu}_{i,j-1}}{2(\Delta\bar{b})^2}$$

$$A_5 = \left[\frac{1}{\mathrm{Re}\ \bar{\rho}\bar{w}^2}\right]_{i+1/2,j} \frac{\bar{\mu}_{i,j}}{2(\Delta\bar{b})^2}$$

$$A_6 = \left[\frac{1}{\mathrm{Re}\ \bar{\rho}\bar{w}^2}\right]_{i+1/2,j} \frac{\bar{\mu}_{i,j+1}}{2(\Delta\bar{b})^2}$$

$$B_1 = \frac{1}{\Delta\bar{s}\ \bar{w}_{i+1,j}}, \quad B_2 = \frac{1}{\Delta\bar{s}\ \bar{w}_{i,j}}$$

$$C = \left[\frac{2\bar{\xi}_n}{\bar{w}\bar{R}} + \frac{(\bar{W}_0)^2}{\bar{\rho}\bar{w}^2\bar{R}}\frac{\partial\bar{\rho}}{\partial\bar{b}} + \frac{2}{\bar{w}^2}\left(\bar{\Omega}_s\frac{\partial\bar{w}}{\partial\bar{s}} + \bar{\Omega}_n\frac{\bar{w}}{\bar{R}} + \bar{\Omega}_b\bar{\xi}_n\right)\right]_{i+1/2,j}$$

Constants B_3, B_4, and C_2 for the difference equation (12*b*) are given by

$$B_3 = \frac{\bar{w}_{i+1,j}}{\Delta\bar{s}}, \quad B_4 = \frac{\bar{w}_{i,j}}{\Delta\bar{s}},$$

$$C_2 = \left[\frac{2\bar{\Omega}_s\bar{w}}{\bar{R}} - 2\bar{\Omega}_n\frac{\partial\bar{w}}{\partial\bar{s}} + \frac{1}{\bar{\rho}^2}\frac{\partial\bar{P}_0}{\partial\bar{s}}\frac{\partial\bar{\rho}}{\partial\bar{b}}\right]_{i+1/2,j}$$

Knowing the value of $(\bar{\xi}_n)_{i+1,j}$, the value of $\bar{\xi}_s$ at the new $\bar{s}$ station can be found from equation (7). The method is stable for all values of the ratio $\Delta\bar{s}/(\Delta\bar{b})^2$, where $\Delta\bar{s}$ and $\Delta\bar{b}$ are the step sizes in s and b directions, respectively. The method converges with discretization error $0\,[(\Delta\bar{s})^2 + (\Delta\bar{b}^2)]$.

Knowing $\bar{\xi}_s$, equation (9) can be solved to derive the values of $\bar{u}$ and $\bar{v}$. Equation (9) is solved by the successive over-relaxation method. The boundary condition is $\bar{\psi} = 0$ along all the wall surfaces. The numerical method uses the following iteration scheme:

$$(\bar{\psi})_{i,j}^{(n+1)} = (\bar{\psi})_{i,j}^{(n)} + \frac{\omega}{4}\left[(\bar{\psi})_{i-1,j}^{(n+1)} + (\bar{\psi})_{i+1,j}^{(n)} + (\bar{\psi})_{i,j-1}^{(n+1)} + (\bar{\psi})_{i,j+1}^{(n)} - 4(\bar{\psi})_{i,j}^{(n)} - h^2(\bar{\xi}_s)_{i,j}\right] \tag{13}$$

where h is the stepsize $h = \Delta\bar{n} = \Delta\bar{b}$ and ω is a relaxation parameter given by

$$\omega = \frac{8 - 4\sqrt{4-\alpha^2}}{\alpha^2}$$

with $\alpha = \cos(\pi/M) + \cos(\pi/N)$ where M and N are, respectively, the total number of increments into which the horizontal, i.e., n, and vertical, i.e., b, sides of the rectangular region are divided. More details of the solution for equation (13) can be found in reference [12].

Initial and Boundary Conditions. The initial conditions at the inlet of the passage are prescribed $[\bar{w}(\bar{b}), \bar{\xi}_{n0}, \bar{\xi}_{s0}, \bar{\rho}(\bar{b})]$, and the angular velocity is known.

The boundary conditions for equations (7) and (8) are as follows. In the inviscid or vortex free region, $\bar{\xi}_s = \bar{\xi}_n = 0$. The boundary conditions on the wall surface for $\bar{\xi}_s$ are derived iteratively from the solution. Initially on the wall, $\bar{\xi}_n = (\bar{\xi}_n)_{\text{inlet}}$ = constant and $\bar{\xi}_s = (\bar{\xi}_s)_{\text{inlet}} + 2\bar{s}/\bar{R}\ (\bar{\xi}_n)_{\text{wall}}$. Thus, the inviscid expression for the secondary vorticity derived by Squire and Winter [2] is prescribed initially. The values of $\bar{\xi}_s$ on the wall surface are continuously updated during the computation. Utilizing these initial boundary conditions, equations (7) and (8) are solved in finite difference form (e.g., equation 12). Knowing $\bar{\xi}_s$ everywhere, equation (9) for $\bar{\psi}$ is solved numerically. Utilizing this zeroth approximation, the boundary condition on the wall surface $[(\bar{\xi}_s)_{\text{wall}}]$ can be updated using the equation

$$(\bar{\xi}_s)_{\text{wall}} = (-7\bar{\psi}_{\text{wall}} + 8\bar{\psi}_{\text{wall}+1} - \bar{\psi}_{\text{wall}+2})/2(\Delta\bar{b})^2$$

where $\bar{\psi}_{\text{wall}+1}$, $\bar{\psi}_{\text{wall}+2}$ represents values at the grid points away from the wall. The first term on the right-hand side is zero. This form is of second-order accuracy [13]. With this new information, values of $\bar{\xi}_s$, $\bar{\psi}$, $\bar{v}$, $\bar{u}$ can be determined. This procedure is repeated until the convergence is achieved. The calculation then proceeds to the next $\bar{s}$ station. The secondary vorticity and secondary flow field throughout the passage is thus determined. The computational flow chart is shown in Fig. 2.

In the present analysis, the boundary condition on the wall for the secondary vorticity is unknown and should come out of the solution. Since the secondary vorticity peaks near the wall, the accuracy of the solution depends on the accuracy of $\bar{\xi}_s$ calculation near the wall. The presence of large gradients in eddy viscosity makes the problem very sensitive to the calculations near the wall. To overcome these difficulties a large number of grid points were chosen near the wall.

Prediction and Comparison With Experimental Data

To check the analysis, assumptions, and numerical technique, the results of the computer program are compared with the following experimental and analytical results.

(*a*) Hawthorne's [14] analytical results.

(*b*) Experimental data from curved duct [2,15].

(*c*) The compressor and turbine cascade data [16,17,18].

(*d*) Model rotors are used to study the effects of rotation and the inlet density stratification.

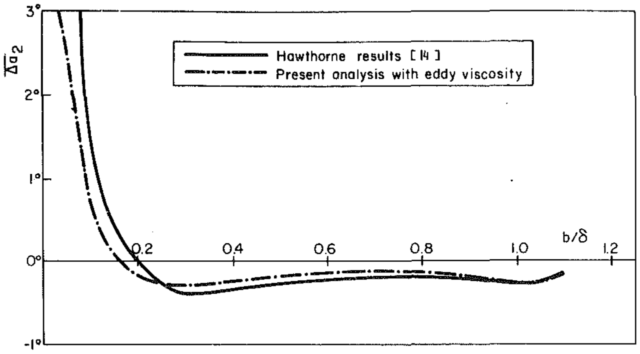

Fig. 3 Comparison between Hawthorne's [14] theoretical results and the predicted change in average outlet angle for $\delta/S = 2$

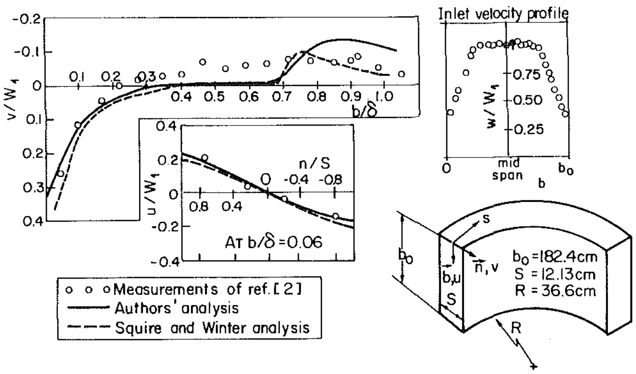

Fig. 4 Comparison between experimental and predicted v, u for Squire and Winter duct [2]

Comparison With Hawthorne's Analytical Results. Hawthorne, using Squire and Winter's expression [2] for the secondary vorticity $[\bar{\zeta}_s = (2\bar{s}/\bar{R})(\bar{\zeta}_n)_{\text{inlet}}]$, solved equation (9) for a duct with a large span using a series expansion technique. He assumes a (1/7)th power boundary layer coming into the duct. The analysis is valid for incompressible, inviscid, homogeneous flow in a non-rotating duct. In this case, the second and third terms in equation (7) and the corresponding terms in equation (8) are zero. He predicts very large secondary vorticity at the wall. The results of Hawthorne are not accurate near the wall, since the viscous effects are neglected. His results are compared with the authors' results for $\overline{\Delta\alpha}_2$ for $\delta/S = 2$ in Fig. 3.

The authors' results agree very well with Hawthorne's inviscid theory away from the wall. The departure between solutions is large (for $b < 0.2\ \delta$) near the wall where the effects of viscosity cannot be neglected. It is thus clear that inviscid analyses are not valid near the wall, and that effects of viscosity should be considered for accurate prediction.

Comparison With Experimental Data From Curved Ducts. Squire and Winter [2] carried out detailed measurements in a curved duct with 94 deg flow turning and a 36.6 cm radius. The width (S) and height of the channel were 12.13 cm and 182.4 cm, respectively. The measured inlet velocity (primary flow) profile as well as the predicted and measured secondary velocity profiles are shown in Fig. 4. In this case, the second and third terms in equation (7) and the corresponding terms in equation (8) are zero. The flow is assumed laminar. The measured values of u (spanwise or b direction) at $b/\delta = 0.06$, which is very near the wall, agree very well with the authors' prediction. The prediction from Squire and Winter's [2] analysis also is shown. This confirms the earlier conclusion that the viscous effects should be included to accurately predict the secondary flow near the wall regions. The prediction of the secondary velocity (v) in the n direction shows good agreement with the data.

Lewkowicz [15] carried out comprehensive measurements

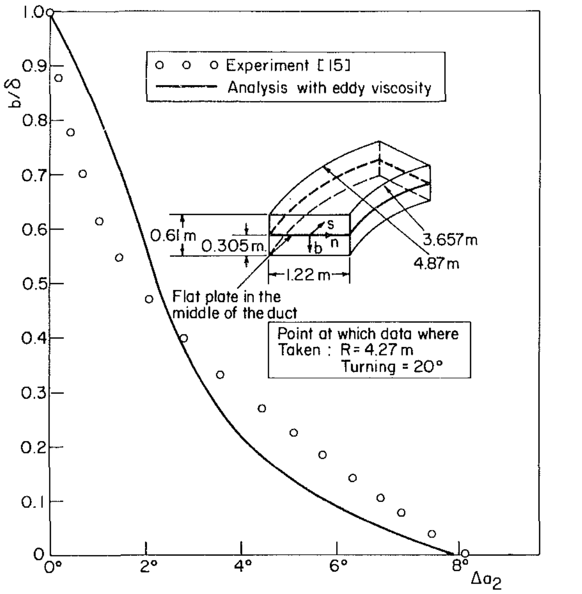

Fig. 5 Comparison between experimental and predicted $\Delta\alpha_2$ for Lewkowicz bend [15]

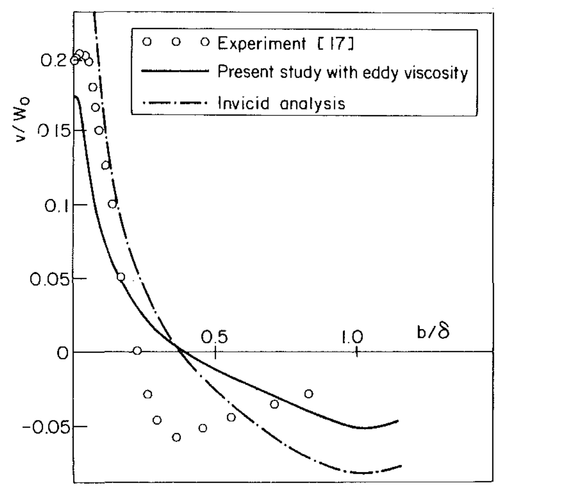

Fig. 6 Comparison between experimental and predicted cross flow velocity profile at the exit of the cascade [17]

in a curved duct shown as insert in Fig. 5. The predicted deviation angle ($\Delta\alpha_2 \approx v/w$) variation across the boundary layer is in excellent agreement with the predictions from the authors' analysis. It is thus evident that the development of cross flow in the three-dimensional boundary layer is predicted accurately from this analysis. Since the turning is small (20 deg) and the radius of the bend is large, this test case falls within the realm of a small cross-flow assumption. Hence, good agreement between the theory and experiment is as expected. The inviscid classical analysis predicts nearly twice the measured $\Delta\alpha_2$ (not shown in Fig. 5).

Comparison With the Compressor and Turbine Cascade Data. The first and fourth terms in equation (7) and the corresponding terms in equation (8) are retained for the prediction of the flow through cascades described in this section.

Papailiou et al. [17] carried out experiments in a compressor cascade consisting of blades with a NACA 65-12-A_{10}-10 profile. Other parameters of the cascade were as follows: inlet free stream velocity = 44.9 m/s, space chord ratio = 0.8, aspect ratio = 2.1, stagger angle = 15 deg, inlet air angle = 20.4 deg, and outlet air angle = −23.8 deg. The experimental results of Papailiou et al. [17] are compared with

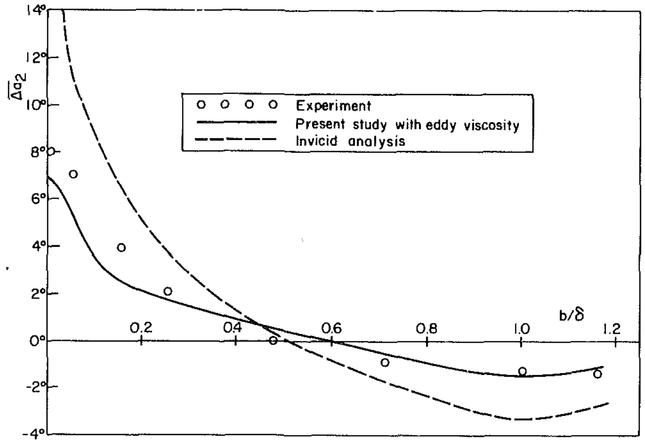

Fig. 7 Comparison between experimental and predicted change in outlet angle for Marchal and Sieverding's cascade [16]

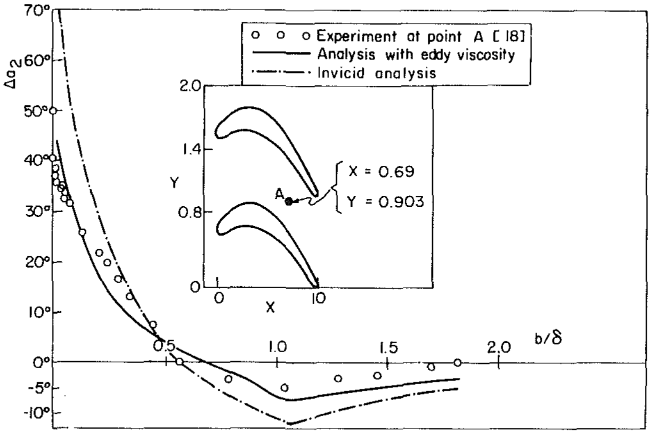

Fig. 8(a) Comparison between experimental and predicted change in angle for Langston's cascade [18]

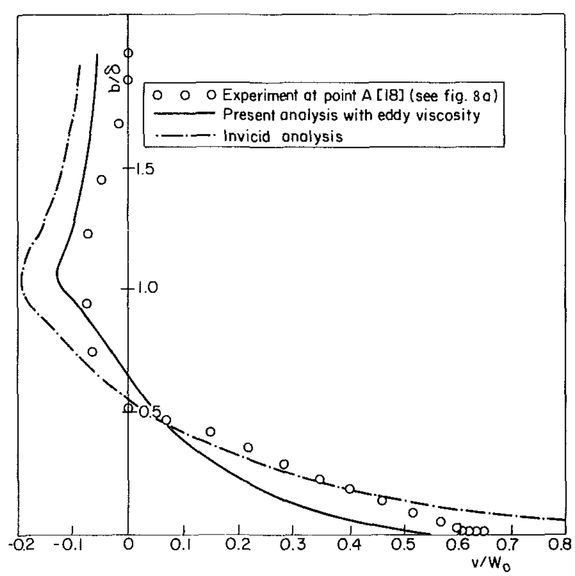

Fig. 8(b) Comparison between experimental and predicted cross flow velocity profiles for Langston's cascade [18]

the results of the present analysis for the secondary velocity v at the exit of the cascade in Fig. 6. The prediction of the present study is better near the wall than the inviscid analysis. This provides a validation of the authors' approach in updating the boundary condition for $(\bar{\zeta}_s)_{\text{wall}}$ near the wall.

Marchal and Sieverding [16] carried out experiments for a turbine cascade. The cascade geometry was as follows: chord = 12 cm, space to chord ratio = 0.725, stagger angle = −42.5 deg, blade height = 10 cm. The inlet and outlet air angles were 0 deg and −67.8 deg, respectively. The Reynolds number based on the chord and the exit velocity was 2.61 × 10^5. The experimental results for $\Delta\alpha_2$ are compared with the predictions of the present analysis and the predictions from the inviscid analysis in Fig. 7. The inviscid analyses provides poor predictions near the wall. The authors' analysis gives much better predictions in the entire flow field.

Langston [18] recently carried out measurements of the subsonic flow in a large-scale rectilinear turbine cascade. The cascade geometry was as follows: chord = 34 cm,

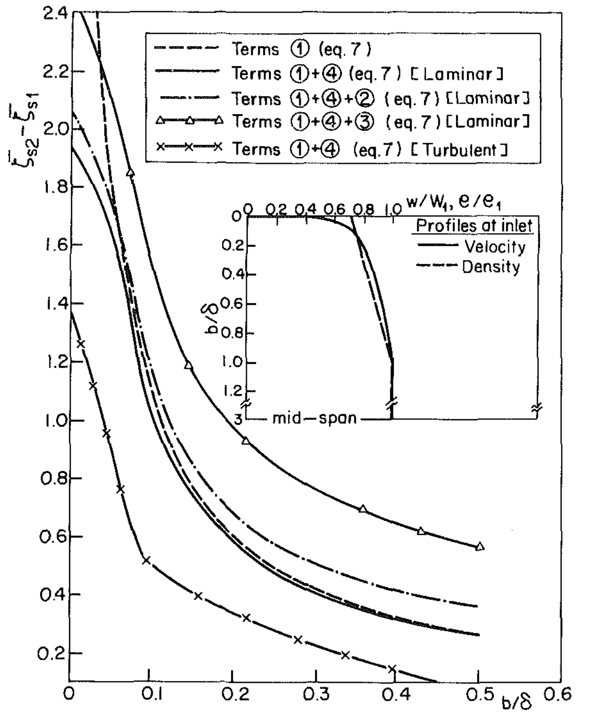

Fig. 9 Relative secondary vorticity at the exit of the model compressor rotor in the casing region

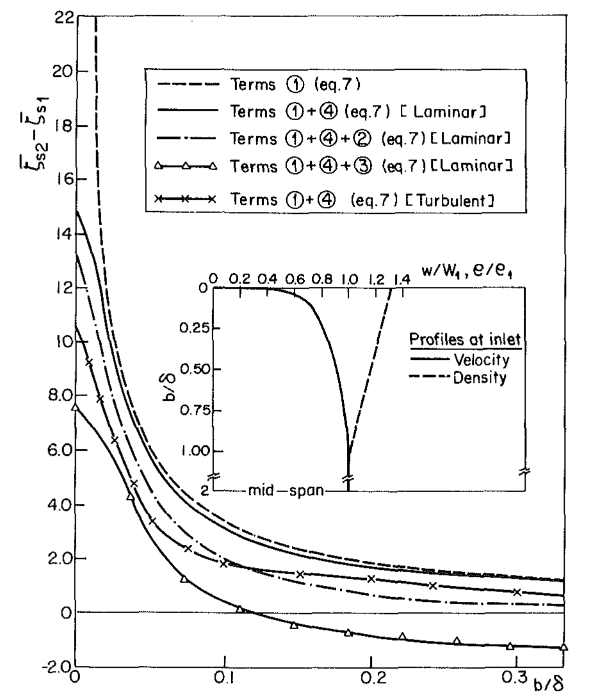

Fig. 10 Relative secondary vorticity at the exit of the model turbine rotor in the casing region

pitch/chord ratio = 0.78, aspect ratio = 0.81, camber angle = 70 deg. The inlet boundary layer thickness, displacement thickness, and momentum thickness were 3.3 cm, 0.376 cm, and 0.279 cm, respectively.

The predictions of the cross-flow velocity and the yaw angle deviation for Langston's [18] cascade is compared with the data in Fig. 8. The measurements at station A (Fig. 8(*a*)) near mid-passage at 69 percent of axial chord are used for this comparison. The results are quite good since this station is away from the suction side of the airfoil, where the separation occurs. The authors' prediction is not valid near a separated flow. The analysis predicts maximum cross flow at the middle of the passage, decaying as we go near the blade surfaces. Langston's measurements show an increase in the cross-flow velocity when going from $Y = 0.903$ to $Y = 0.766$. The present analysis gives much better results than the inviscid analysis near the wall.

Model Rotors. Calculations have been made for a model compressor rotor and a model turbine rotor in order to study the effect of rotation and density stratification on the development of relative secondary vorticity. The model rotors have the following features. Compressor rotor: $\beta_1 = 40$ deg, $\beta_2 = 10$ deg, $\lambda = 25$ deg, $W_2/W_1 = 0.78$, $2\delta/b_0 = 0.33$, $\Omega\delta/W_1 = 0.188$. Turbine rotor: $\beta_1 = 20$ deg, $\beta_2 = -70$ deg, $\lambda = 25$ deg, $W_2/W_1 = 2.74$, $2\delta/b_0 = 0.75$, $\Omega\delta/W_1 = 0.56$.

The velocity and density profiles employed in this computation are shown as inserts in Figs. 9 and 10 for the compressor and turbine rotors, respectively. The assumed density profile for a compressor rotor (Fig. 9) is of the type encountered in thermal boundary layers near the hub and annulus walls. The density profile for the turbine (Fig. 10) represents the non-uniformity in temperature at the exit of the combustion chamber. The assumed magnitude and profiles of velocity and density are arbitrary.

The contribution to the secondary vorticity development in a compressor rotor from various terms in equation (7) is shown in Fig. 9. The laminar viscous term has a dominant effect near the wall. The turbulence reduces the secondary vorticity drastically across the entire boundary layer. The rotation and density stratification have appreciable influence in this case. It should be remarked here that the contribution due to the density stratification will be reversed if the density gradients are opposite to those shown in Fig. 9. Such a case may occur due to inherent design features of the preceding blade row. A similar trend is observed in the case of a turbine rotor as shown in Fig. 10. The dominant effect of the term $\Omega_n \partial w/\partial s$ is evident from this figure. The rotation effect is opposite to those of a compressor for this particular case.

Concluding Remarks

The present analysis employs the classical approach of uncoupled primary and secondary flow fields so it cannot predict any transport of the secondary vorticity and subsequent roll up near the suction side of the passage. However, it goes beyond the classical approach by introducing the effects of viscosity, rotation, and density stratification on the development of secondary vorticity.

The agreement between the analysis and several sets of data in a duct, compressor, and turbine cascade is good in all regions. Earlier theories had poor predictions near the wall (up to approximately 2/10 of the boundary layer), and this has been rectified by introducing the viscous effects on secondary flow and vorticity development. Excellent agreement between experimental data and the present analysis near the wall emphasizes not only the need for a viscous analysis for accurate prediction, but also confirms the validity of the method of updating of the boundary condition developed in this paper.

The present method can be improved by allowing for the change in the streamwise velocity and development of the wall boundary layers.

Acknowledgments

This work was sponsored by the National Aeronautics and Space Administration through the grant NSG 3212, with Dr. P. Sockol as the Technical Monitor. The authors wish to thank Dr. J. Galmes for his help in the derivation of the vorticity equation for turbulent flow (Appendix 1).

References

1 Hawthorne, W. R., "Secondary Circulation of Fluid Flow," *Proceedings of the Royal Society*, Series A, Vol. 206, 1951, p. 374.

2 Squire, H. B., and Winter K. G., "The Secondary Flow in a Cascade of Airfoils in a Non-Uniform Stream," *Journal of Aeronautical Sciences*, Vol. 18, 1951, p. 271.

3 Horlock, J. H., and Lakshminarayana, B., "Secondary Flows: Theory, Experiment, and Application in Turbomachinery Aerodynamics," *Annual Review of Fluid Mechanics*, Vol. 5, 1973, pp. 247–280.

4 Lakshminarayana, B., and Horlock, J. H., "Effect of Shear Flows on Outlet Angle in Axial Flow Compressor Cascades," ASME *Journal of Basic Engineering*, Vol. 89, 1967, pp. 191–200.

5 Barber, T. J., "Analysis of Shearing Internal Flows," AIAA Paper 81-0005, Jan. 1981.

6 Abdallah, S., and Hamed, A., "An Inviscid Solution for the Secondary Flow in Curved Ducts," AIAA Paper 80-1116, 1980.

7 Pratrap, V. S., and Spalding, D. B., "Fluid Flow and Heat Transfer in Three-Dimensional Duct Flows," *International Journal of Heat and Mass Transfer*, Vol. 19, 1976, pp. 1183–1188.

8 Briley, W. R., and McDonald, H., "Computation of Three-Dimensional Turbulent Subsonic Flow in Curved Passages," UARL Report R75-911596-8, 1975.

9 Briley, W. R., and McDonald, H., "Analysis and Computation of Viscous Subsonic Primary and Secondary Flows," AIAA Paper 79-1453, 1979.

10 Lakshminarayana, B., and Horlock, J. H., "Generalized Expressions for Secondary Vorticity Using Intrinsic Coordinates," *Journal of Fluid Mechanics*, Vol. 59, Part 1, 1973, pp. 97–115.

11 Schlichting, H., *Boundary Layer Theory*, Seventh Edition, McGraw-Hill.

12 Chow, Chuen-Yen, *An Introduction to Computational Fluid Mechanics*, Wiley, 1979.

13 Roache, P. J., *Computational Fluid Dynamics*, Hermosa Publishers, 1972.

14 Hawthorne, W. R., "Some Formulas for the Calculation of Secondary Flows in Cascades," British Aeronautical Research Council Report 17519, 1955.

15 Lewkowicz, A. K., "Two- and Three-Dimensional Incompressible Turbulent Boundary Layers," Ph.D. thesis, University of Liverpool, 1965.

16 Marchal, Ph., and Sieverding, C. H., "Secondary Flows Within Turbomachinery Bladings," AGARD CP 214, 1977.

17 Papailiou, K., Flot, R., and Mathieu, J., "Secondary Flows in Compressor Bladings," ASME Paper 76-GT-57, 1976.

18 Langston, L. S., "Crossflows in a Turbine Cascade Passage," ASME *Journal of Engineering for Power*, Vol. 102, Oct. 1980, pp. 866–874.

APPENDIX 1

Vorticity Equation for Turbulent Flow

The Reynolds equation for a turbulent flow field is given by

$$(\mathbf{V}\cdot\nabla)\mathbf{V}+\overline{(\mathbf{u}'\cdot\nabla)\mathbf{u}'}=-\frac{\nabla P}{\rho}-\frac{\mu}{\rho}\nabla\times(\nabla\times\mathbf{V})+\frac{4}{3}\mu\nabla(\nabla\cdot\mathbf{V}) \qquad \text{(A1)}$$

where, $\mathbf{V}$ is the mean velocity vector and $\mathbf{u}'$ is the fluctuating velocity vector.

The vorticity equation can be derived by taking the curl of equation (A1). All the terms in equation (A1) except the expression $[\overline{(\mathbf{u}'\cdot\nabla)\mathbf{u}'}]$ are expanded in reference [10]. Expansion of this term follows.

The fluctuating velocity vector is written as,

$$\mathbf{u}'=q_s'\mathbf{s}+q_n'\mathbf{n}+q_b'\mathbf{b}$$

where q_s', q_n', q_b' are fluctuating components in s, n, b directions. Hence,

$$\overline{(\mathbf{u}'\cdot\nabla)\mathbf{u}'}=\overline{q_s'\frac{\partial\mathbf{u}'}{\partial s}}+\overline{q_n'\frac{\partial\mathbf{u}'}{\partial n}}+\overline{q_b'\frac{\partial\mathbf{u}'}{\partial b}} \tag{A2}$$

Expanding the above expression in intrinsic coordinate system [10] and assuming that the flow is incompressible, it can be proved

$$\overline{(\mathbf{u}'\cdot\nabla\mathbf{u}')}=\mathbf{s}\left[\frac{\partial}{\partial s}(\overline{q_s'^2})+\frac{\partial}{\partial n}(\overline{q_s'q_n'})+(\overline{q_s'q_b'})-\frac{\overline{q_s'q_n'}}{R}\right]$$

$$+\mathbf{n}\left[\frac{\overline{q_s'^2}}{R}+\frac{\partial}{\partial s}(\overline{q_s'q_n'})+\frac{\partial}{\partial n}(\overline{q_n'^2})+\frac{\partial}{\partial b}(\overline{q_n'q_b'})\right.$$

$$\left.-\overline{q_s'q_b'}\frac{1}{\tau}+\overline{q_n'q_s'}\left(\frac{1}{a_n}\frac{\partial a_n}{\partial s}\right)\right]+\mathbf{b}\left[\frac{\partial}{\partial s}(\overline{q_s'q_b'})\right.$$

$$+\frac{\partial}{\partial n}(\overline{q_n'q_b'})+\frac{\partial}{\partial b}(\overline{q_b'^2})+\overline{q_s'q_n'}\frac{1}{\tau}$$

$$\left.+\overline{q_b'q_s'}\frac{1}{a_b}\frac{\partial a_b}{\partial s}\right]$$

The above expression is simplified by assuming that τ and R are very large, and by neglecting all terms involving derivatives in the streamwise and normal direction. The final result is

$$\overline{(\mathbf{u}\cdot\nabla\mathbf{u}')}\approx\mathbf{s}\frac{\partial}{\partial b}(\overline{q_s'q_b'})+\mathbf{n}\frac{\partial}{\partial b}(\overline{q_n'q_b'})+\mathbf{b}\left(\frac{\partial}{\partial b}\overline{q_b'^2}\right) \tag{A3}$$

Taking the curl of the above quantity and utilizing the assumptions made earlier, equation (A3) simplifies to,

$$\overline{(\mathbf{u}'\cdot\nabla\mathbf{u}')}=-\mathbf{s}\frac{\partial^2}{\partial b^2}(\overline{q_n'q_b'})+\mathbf{n}\frac{\partial^2}{\partial b^2}(\overline{q_s'q_b'}) \tag{A4}$$

The terms $(\overline{q_n'q_b'})$ and $(\overline{q_s'q_b'})$ can be modeled using the eddy viscosity concept

$$\overline{q_n'q_b'}=-\frac{\mu_e}{\rho}\frac{\partial v}{\partial b}\ ,\ \overline{q_s'q_b'}=-\frac{\mu_e}{\rho}\frac{\partial w}{\partial b} \tag{A5}$$

The secondary vorticity can be written as,

$$\zeta_s=\frac{\partial u}{\partial n}-\frac{\partial v}{\partial b}$$

In most of the cases $\partial v/\partial b >> \partial u/\partial n$, hence $\zeta_s\approx-\partial v/\partial b$. Since $\partial w/\partial b=\zeta_n$, the correlations in equation (A5) can be expressed as

$$\overline{q_n'q_b'}=\frac{\mu_e}{\rho}\zeta_s\ ,\ q_s'q_b'=-\frac{\mu_e}{\rho}\zeta_n \tag{A6}$$

Substituting expressions (A6) in equation (A4) it follows that

$$\overline{(\mathbf{u}'\cdot\nabla\mathbf{u}')}=-\mathbf{s}\frac{\partial^2}{\partial b^2}\left(\frac{\mu_e}{\rho}\zeta_s\right)-\mathbf{n}\frac{\partial^2}{\partial b^2}\left(\frac{\mu_e}{\rho}\zeta_n\right) \tag{A7}$$

Transferring these terms to the right-hand side of equation (A2), the additional terms that appear on the right-hand side of equations (A5) and (A6) are, respectively,

$$\left[\frac{1}{w^2}\frac{\partial^2}{\partial b^2}\left(\frac{\mu_e}{\rho}\zeta_s\right)\right]\qquad\left[\frac{\partial^2}{\partial b^2}\left(\frac{\mu_e}{\rho}\zeta_n\right)\right] \tag{A8}$$